29
2-27-80

ornl

OAK
RIDGE
NATIONAL
LABORATORY

UNION
CARBIDE

OPERATED BY
UNION CARBIDE CORPORATION
FOR THE UNITED STATES
DEPARTMENT OF ENERGY

ORNL/TM-7116

Solidification Behavior of Austenitic Stainless Steel Filler Metals

S. A. David
G. M. Goodwin
D. N. Braski

ORNL/TM-7116

Contract No W-7405-eng-26

METALS AND CERAMICS DIVISION

SOLIDIFICATION BEHAVIOR OF AUSTENITIC STAINLESS STEEL FILLER METALS

S. A. David, G. M. Goodwin, and D. N. Braski

Date Published: February 1980

OAK RIDGE NATIONAL LABORATORY
Oak Ridge, Tennessee 37830
operated by
UNION CARBIDE CORPORATION
for the
DEPARTMENT OF ENERGY

CONTENTS

SOLIDIFICATION BEHAVIOR OF AUSTENITIC STAINLESS STEEL FILLER METALS

S. A. David, G. M. Goodwin, and D. N. Braski

ABSTRACT

Thermal analysis and interrupted solidification experiments on selected austenitic stainless steel filler metals provided an understanding of the solidification behavior of austenitic stainless steel welds. The sequences of phase separations found were for type 308 stainless steel filler metal, $L \rightarrow L + \delta \rightarrow L + \delta + \gamma \rightarrow \gamma + \delta$, and for type 310 stainless steel filler metal, $L \rightarrow L + \gamma \rightarrow \gamma$.

In type 308 stainless steel filler metal, ferrite at room temperature was identified as either the untransformed primary δ-ferrite formed during the initial stages of solidification or the residual ferrite after Widmanstätten austenite precipitation. Microprobe and scanning transmission electron microscope microanalyses revealed that solute extensively redistributes during the transformation of primary δ-ferrite to austenite, leading to enrichment and stabilization of ferrite by chromium. The type 310 stainless steel filler metal investigated solidifies by the primary crystallization of austenite, with the transformation going to completion at the solidus temperature. In our samples residual ferrite resulting from solute segregation was absent at the intercellular or interdendritic regions.

INTRODUCTION

Austenitic stainless steels form an important class of materials in several energy systems. Austenitic stainless steel weld metal normally has a duplex structure that contains varying amounts of ferrite. During the past three decades the subject of ferrite in austenitic stainless steel has received and continues to receive much attention.[1-4] It is recognized that if sufficient ferrite is in the weld, the ferrite will effectively prevent hot cracking.[5-7] Several theories have been advanced to explain this phenomenon,[5-11] yet to date our understanding of hot cracking is still incomplete. Before the beneficial effect of δ-ferrite in reducing hot cracking can be established, we need to understand the origin of duplex structure in austenitic stainless steel weld

metal. Extensive discussions have been published on the solidification behavior and origin of ferrite in austenitic stainless steel weld metal, but no one has been able to clearly establish the solidification sequences leading to the observed final microstructure of the weld metal.

A vertical section[12] (at 70 wt % Fe) of the ternary equilibrium system Fe-Cr-Ni (Fig. 1) shows possible sequences of phase separation during solidification under equilibrium conditions for various alloy compositions. However, we should point out that the solidification behavior and sequences of phase separation in austenitic stainless steel weld metal depart considerably from the phase diagram as a result of the presence of other alloying elements and the rapid cooling of the weld metal. Generally, austenitic stainless steel weld metal solidifies by primary

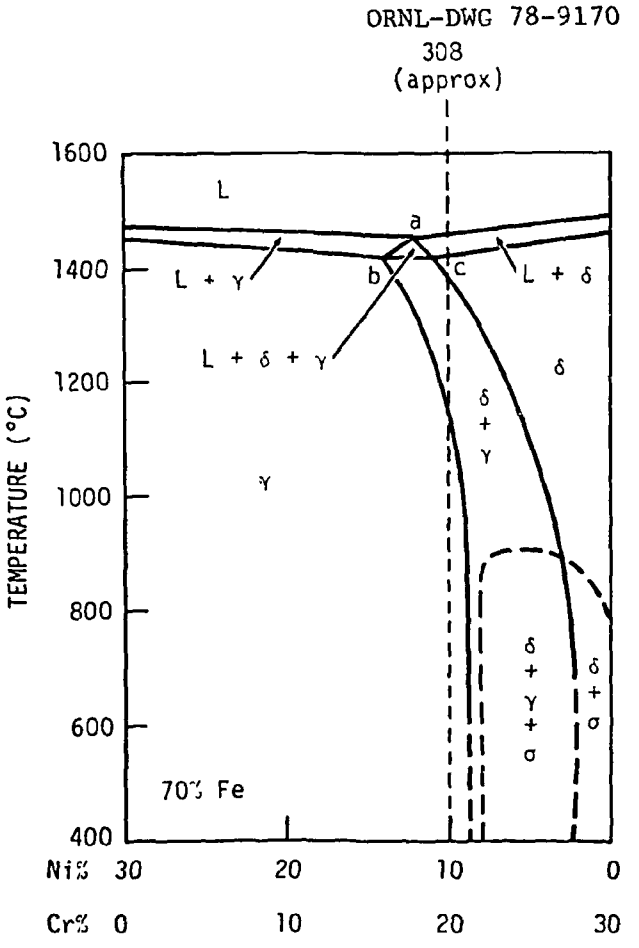

Fig. 1. Vertical Section (at 70 wt % Fe) of Ternary Equilibrium System Fe-Cr-Ni. Based on I. Masumoto, K. Tamaki, and M. Kutsuma, *Yosetsu Gakkai-Shi*, 41(11): 1306–14 (1972).

separation of austenite or ferrite from the melt. In certain cases after ferrite forms austenite can envelop the ferrite and thus interrupt its growth.

Our purpose was to examine in detail the solidification behavior of austenitic stainless steels of compositions on either side of the triangle of three-phase equilibrium in Fig. 1 and to establish the origin of ferrite in the duplex structure of austenitic stainless steel weld metal. We designed thermal analysis and interrupted solidification experiments to correlate the observed microstructural features and solute distribution with solidification behavior.

EXPERIMENTAL PROCEDURE

DTA and Interrupted Solidification

Differential Thermal Analysis (DTA) was carried out in argon in a Mettler Thermoanalyzer. A sample weighing 7 to 8 g was heated to about 50°C above the presumed liquidus temperature of the sample and then cooled at a constant rate of about 6°C/min. Compositions of the alloys investigated are given in Table 1. During cooling a 12-channel compensated recorder traced the DTA curves.

We conducted interrupted solidification experiments by heating the sample in argon to a temperature above its liquidus in a vertical tube furnace, slowly cooling the sample to a predetermined temperature below the liquidus, and quenching the sample in an ice bath. The progress of

Table 1. Austenitic Stainless Steel Filler Metal Compositions[a]

Alloy	Composition, wt %						
	C	Mn	Si	P	S	Cr	Ni
308	0.065	1.52	0.44	0.022	0.008	20.51	10.53
310	0.110	1.64	0.50	0.014	0.009	26.73	21.15

[a]Balance iron.

solidification was followed by metallographically analyzing the samples quenched from a series of temperatures within the freezing range of the alloy. To compare the results of the interrupted solidification experiments with those of typical welds, gas tungsten-arc (GTA) bead-on-plate welds were made with the same filler metals used for the above investigations.

We used standard metallographic techniques for austenitic stainless steels for microstructural analysis. The samples were etched with a solution containing five parts concentrated HCl to one part concentrated HNO_3.

Microanalysis

A few secondary dendrite arms in the samples were traversed by microprobe analysis. We plotted ratios of the intensity at different points to the intensity of the pure element as a function of distance.

A scanning transmission electron microscope (STEM) with an energy-dispersive x-ray spectrometer was used to analyze for microsegregation of the constituent elements within the ferrite network.[13-14] Foils of type 308 stainless steel specimens were electropolished with a dual jet polishing apparatus and a solution of 10 vol % perchloric acid in methanol. The samples were polished at −10°C with 55 V dc. Composition profiles were determined by manually traversing the foil in steps of either 0.2 or 0.1 μm and collecting x-ray spectra at each point for 60 s. The weight fractions of the major alloying elements iron, chromium, and nickel were determined by using the background-corrected integrated intensities of their respective Kα lines, a Fe—16.17% Cr—16.5% Ni foil standard, and the following equations from Cliff and Lorimer:[15]

$$\frac{C_{Cr}}{C_{Fe}} = K_{CrFe} \frac{I_{Cr}}{I_{Fe}} , \qquad (1)$$

$$\frac{C_{Ni}}{C_{Fe}} = K_{NiFe} \frac{I_{Ni}}{I_{Fe}} , \qquad (2)$$

and

$$C_{Cr} + C_{Fe} + C_{Ni} + R = 1 \ , \qquad (3)$$

where C_{Cr}, C_{Fe}, and C_{Ni} are weight fractions of the elements; I_{Cr}, I_{Fe}, and I_{Ni} are the background-corrected $K\alpha$ peak intensities; K_{CrFe} and K_{NiFe} are constants determined from the standard; and P is the weight fraction of the remaining alloy elements. Error bars defining 95% confidence intervals by Student t-tests for the true average percent of the element were determined from sets of measurements made on the standard sample.

RESULTS AND DISCUSSION

Differential Thermal Analysis

Results of DTA on the types 308 and 310 stainless steel filler metal samples (Fig. 2) established the freezing range for the alloys investigated. From the heating and cooling DTA thermograms for the type 308 stainless steel sample three temperatures were identified. For convenience the temperatures are shown on the cooling thermogram.

1. the primary crystallization of δ-ferrite at approximately 1435°C,
2. the start of austenite formation and envelopment of δ-ferrite at 1387°C, and
3. the solidus temperature at about 1355°C.

The above temperatures, except for the liquidus, are slightly different from the values in a previous paper,[4] which used a higher cooling rate (20°C/min) to obtain the thermogram. The temperatures of these multiphase reactions were reproducible within ±2°C. The DTA results also indicate that for type 308 stainless steel filler metal the alloy line position based on nickel and chromium contents alone (shown in Fig. 1) does not represent the actual solidification sequences of the filler metal. The presence of other alloying elements and the nonequilibrium cooling rates employed have considerably changed the alloy line position relative to the phase diagram such that the line now partly traverses the triangle of three-phase equilibrium. This is further confirmed by the interrupted solidification experiments discussed later.

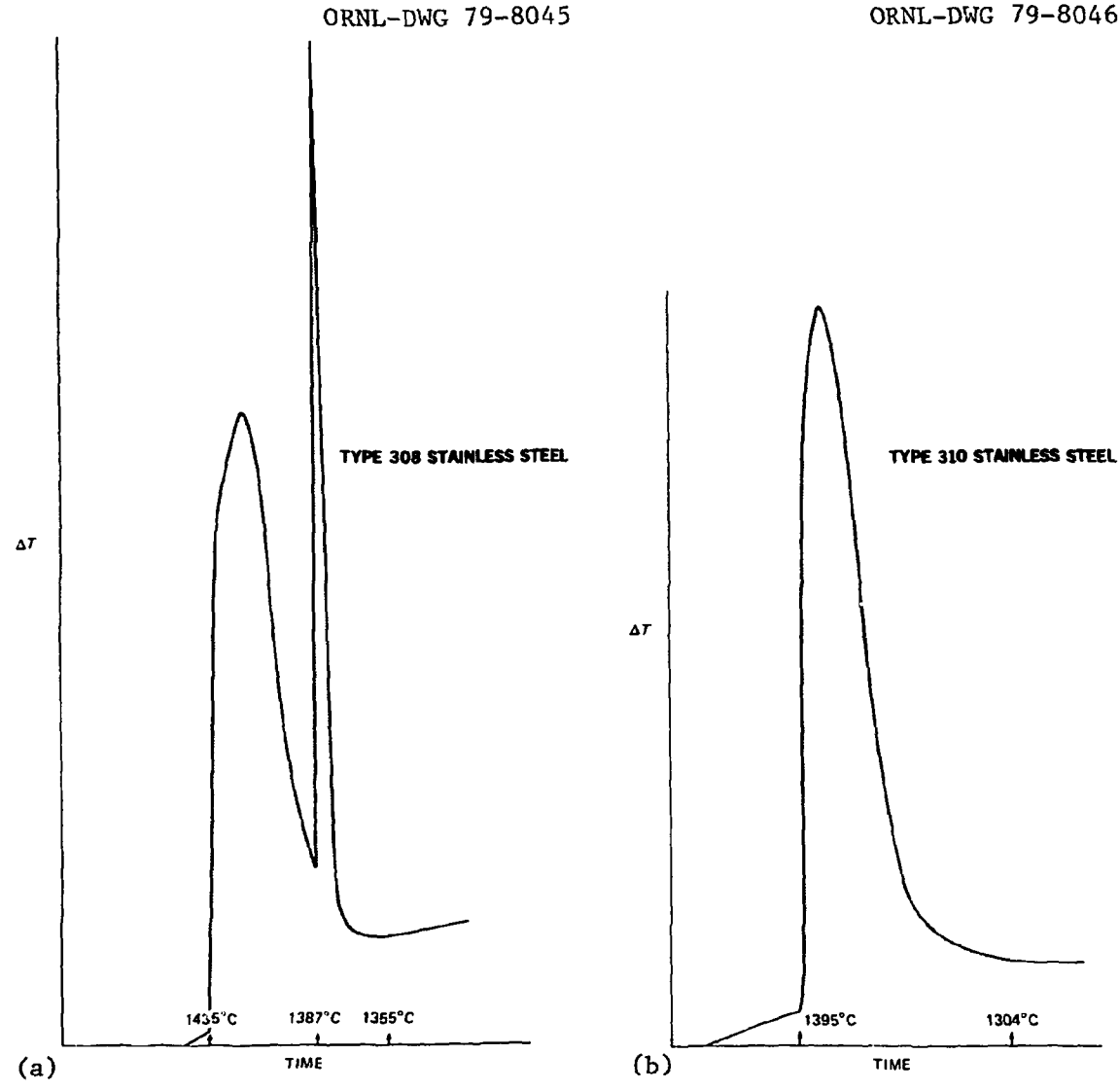

Fig. 2. DTA Curves at Cooling Rate of 6°C/min. (a) Type 308 austenitic stainless steel filler metal. (b) Type 310 filler metal.

Two temperatures were identified from the DTA curves for type 310 stainless steel filler metal:

1. the primary crystallization of austenite (γ) at 1395°C and
2. the solidus temperature at about 1304°C.

The alloy line position describing the solidification path for type 310 stainless steel filler metal would be located to the left of the triangle of three-phase equilibrium (Fig. 1) but in a different vertical section of the ternary diagram.

Solidification Microstructure of Type 308 Stainless Steel Filler Metal

As described earlier, solidification sequences in type 308 stainless steel filler metal include primary crystallization of δ-ferrite with subsequent envelopment by austenite.

Figure 3 shows samples quenched from various temperatures below the liquidus. Primary δ-ferrite forms on cooling the sample to a temperature just below the liquidus (a). Here the dark-etching blocky phase is the primary δ-ferrite. The fine structure surrounding the primary phase indicates that the rest of the area was liquid at the moment of quenching. The ferrite appears dark mainly from the transformation of what was primary δ-ferrite to Widmanstätten austenite. Fredriksson[16] observed similar behavior in 18-8 stainless steel ingots. The volume fraction of the primary δ-ferrite continues to increase as the temperature decreases below the liquidus. However, at 1387°C austenite envelops the primary δ-ferrite as seen in Fig. 3(b) for material quenched from 1365°C. The transformed ferrite enveloped by austenite is shown in Fig. 4. Magnetic etching identified the dark phase in the photomicrograph as δ-ferrite. The transformation of δ-ferrite to Widmanstätten austenite clearly marks the boundary between primary ferrite and austenite at the time of quenching. From the point of complete envelopment further transformations — $L \rightarrow \gamma$ and $\delta \rightarrow \gamma$ — proceed at the γ-L and γ-δ interfaces. As the sample cools to a temperature slightly below that of the solidus (1355°C), the transformation at the γ-L interface goes to completion, leaving behind a skeletal network of untransformed δ-ferrite along the core of the primary and secondary dendrite arms [Fig. 3(c)]. This residual ferrite appears to be very stable on quenching. Interdendritic ferrite resulting from solute segregation was absent from the samples examined. Additionally, the amount of residual δ-ferrite decreased further when the sample was cooled slowly from solidus to room temperature. In view of the extensive solid-state diffusion called for in the above discussion, we should point out that the sequences of solidification and solid-state transformations that occur in the interrupted solidification are more likely to occur in high-heat-input and high-deposition-rate welds.

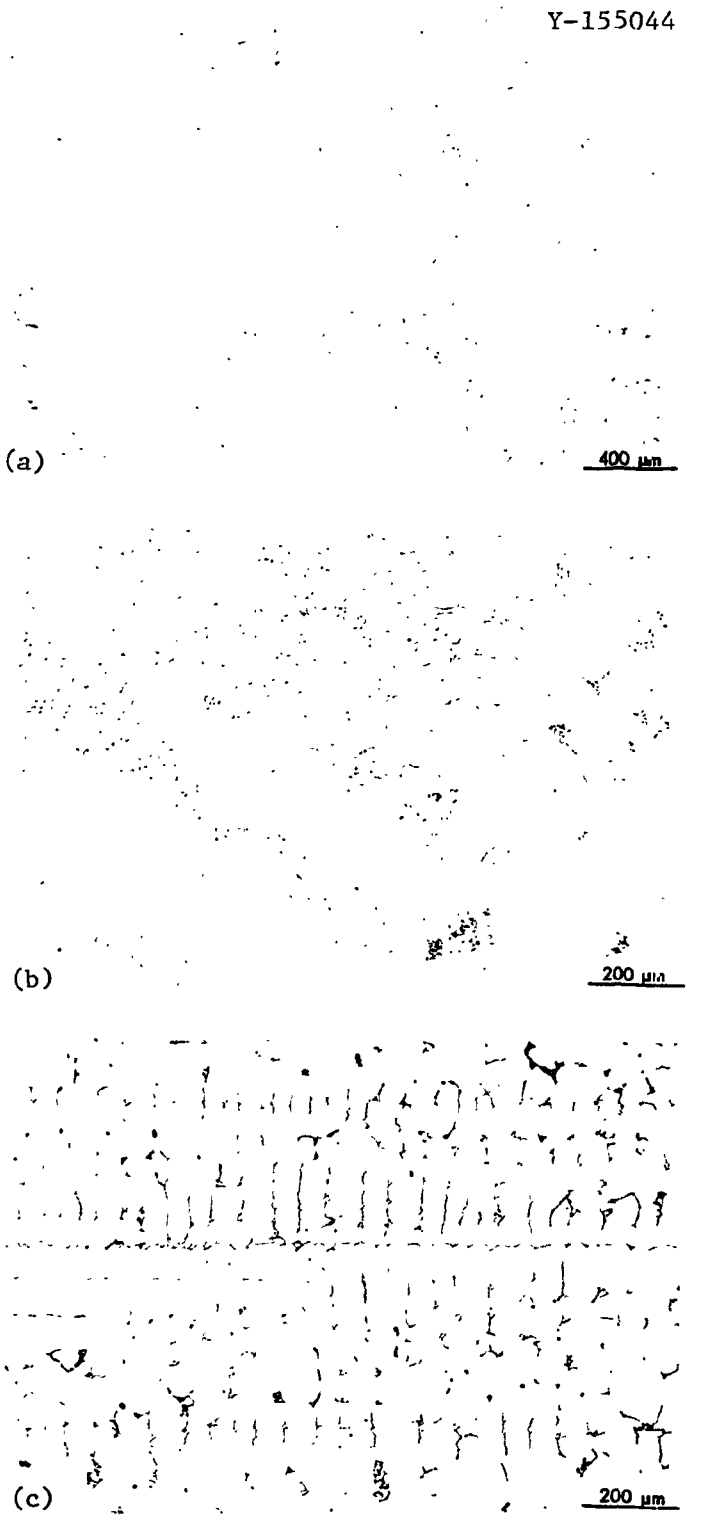

Fig. 3. Interrupted Solidification on Samples of Type 308 Stainless Steel Filler Metal Quenched from (a) 1430°C, (b) 1365°C, and (c) 1335°C.

Fig. 4. Interrupted Solidification Sample Quenched from 1365°C.

Solute Distribution

Figure 5 shows the distribution of Cr, Ni, Si, and Mn across secondary dendrite arms by electron microprobe analysis in the same area of the sample shown in Fig. 3(a). Point count technique showed that the primary δ-ferrite regions contained approximately 2 wt % more chromium and 2 wt % less nickel than the austenite. The distributions of manganese and silicon were fairly uniform. Figure 6 shows the distribution of Cr, Ni, Si, and Mn across a ferrite arm in the same area of the sample as shown in Fig. 3(c). The ferrite regions contained approximately 5 wt % more chromium and 4 wt % less nickel than the austenite. Apparently, the level of chromium seems to have increased significantly in the ferrite while that of nickel decreased during the $\delta \rightarrow \gamma$ transformation.

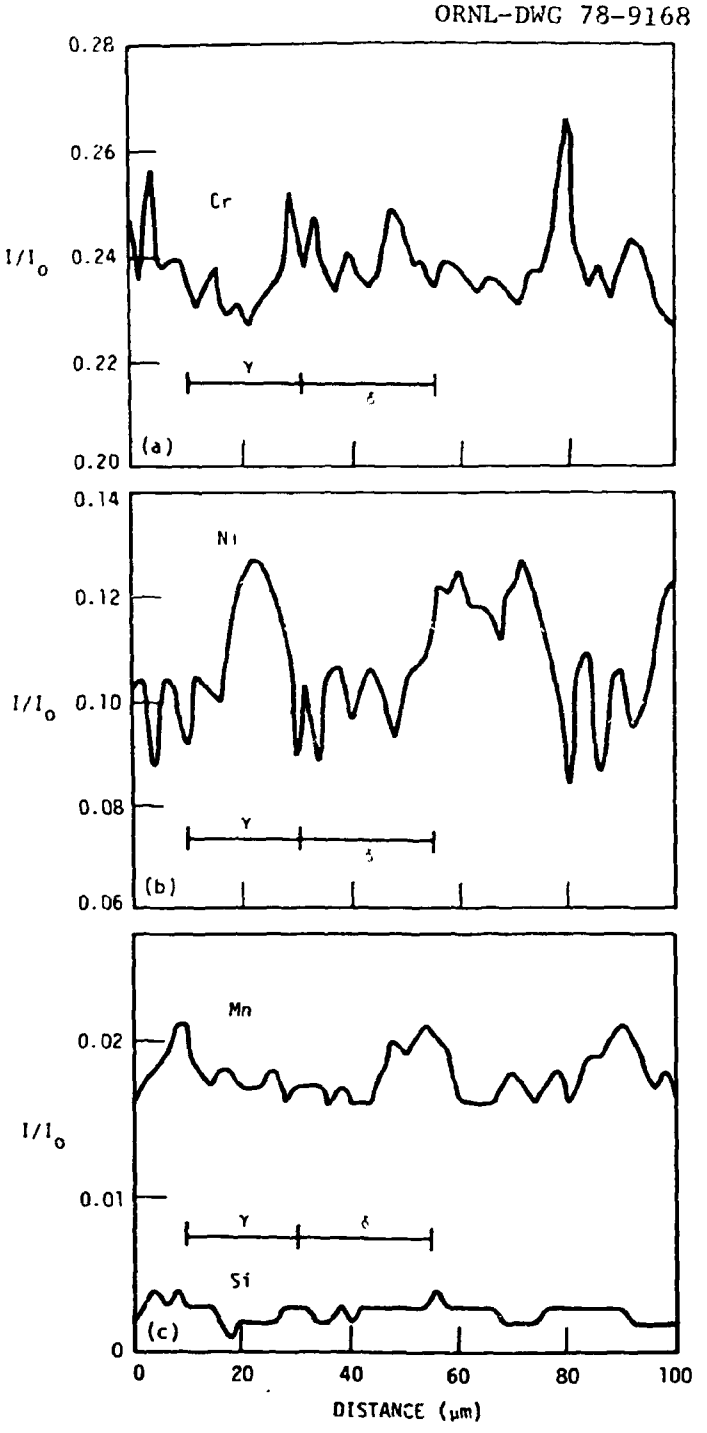

Fig. 5. Distribution of (a) Chromium, (b) Nickel, and (c) Silicon and Manganese Across Secondary Dendrite Arms in the Same Area of the Sample as Shown in Fig. 3(a).

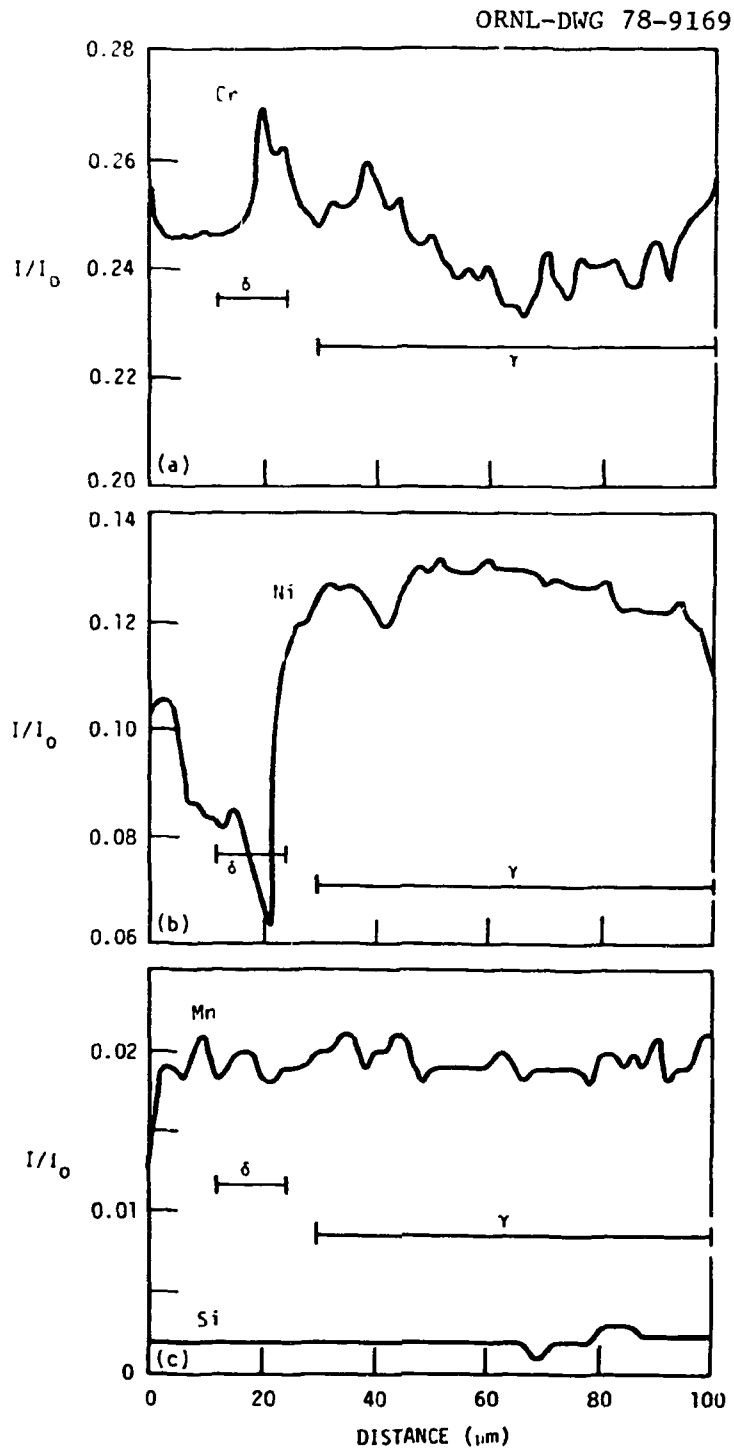

Fig. 6. Distribution of (a) Chromium, (b) Nickel, and (c) Silicon and Manganese Across Secondary Dendrite Arms in the Same Area of the Sample as Shown in Fig. 3(c).

Figure 7(a) shows a transmission electron microscope (TEM) micrograph of a typical region in an interrupted solidification sample [Fig. 3(c)] analyzed by a STEM microanalyzer. Figure 7(b) shows the solute profile across a ferrite network. We should point out that the observed solute profile is that quenched in during the $\delta \rightarrow \gamma$ transformation, at a temperature slightly below the solidus. The average chromium and nickel contents in the austenite are about 21 and 9.5 wt %, respectively, and in the ferrite are about 26 and 7 wt %, respectively. The quenched in-solute profile across the ferrite network also shows chromium peaks on either ferrite side of the $\delta-\gamma$ interface. This peak in chromium level may be attributed to the chromium partitioning to the δ-side of the boundary by fast transport across the interface.[14] Compared with the level of chromium in the primary δ-ferrite from the microprobe results, the level of chromium in the residual ferrite is high. This high level can also be attributed to the transport of partitioned chromium in δ-ferrite, with further redistribution within the ferrite by volume diffusion during $\delta \rightarrow \gamma$ transformation. This high level of chromium seems to stabilize the ferrite and thus prevent it from transforming to Widmanstätten austenite during the quench, as discussed earlier.

The sample quenched from 1365°C [Fig. 3(b)] which contains a network of Widmanstätten austenite and ferrite (Fig. 4), was analyzed by scanning transmission electron microscopy. This revealed another mode by which the structure retains δ-ferrite. The micromorphology of the ferrite is acicular, which differs from the structure described earlier, and the ferrite is much finer. Since primary δ-ferrite transformed to Widmanstätten austenite during the quench, the cooling rate encountered by the sample would be close to that of the weld metal. Hence, the network of austenite and ferrite would be typical of weld metal; in fact, it has been observed in welds. A transmission electron micrograph of a typical region analyzed by the STEM x-ray method is shown in Fig. 8(a). Figure 8(b) shows the solute profile across ferrite in the network. The average chromium and nickel contents in the austenite are 20 and 10 wt %, respectively, and in the ferrite 28 and 5 wt %, respectively. The observed modulation in structure and composition observed throughout the transformed primary δ-ferrite is a result of nucleation of austenite precipitate at the $\delta-\gamma$ boundary and further growth into the ferrite.

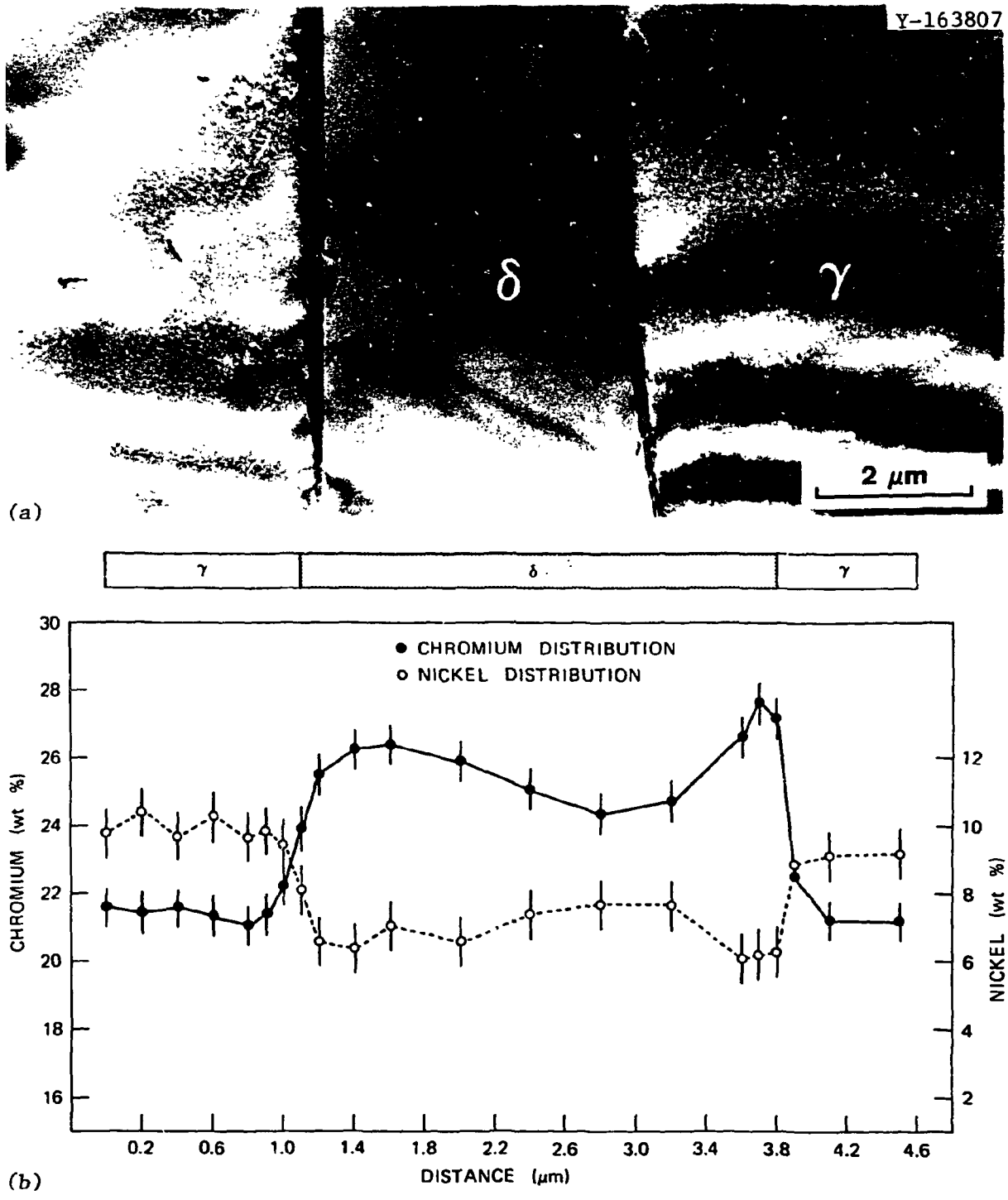

Fig. 7. Scanning Transmission Electron Microanalysis of δ-Ferrite in an Interrupted Solidification Sample Quenched from 1335°C. (a) Transmission electron. (b) Solute profile across the ferrite.

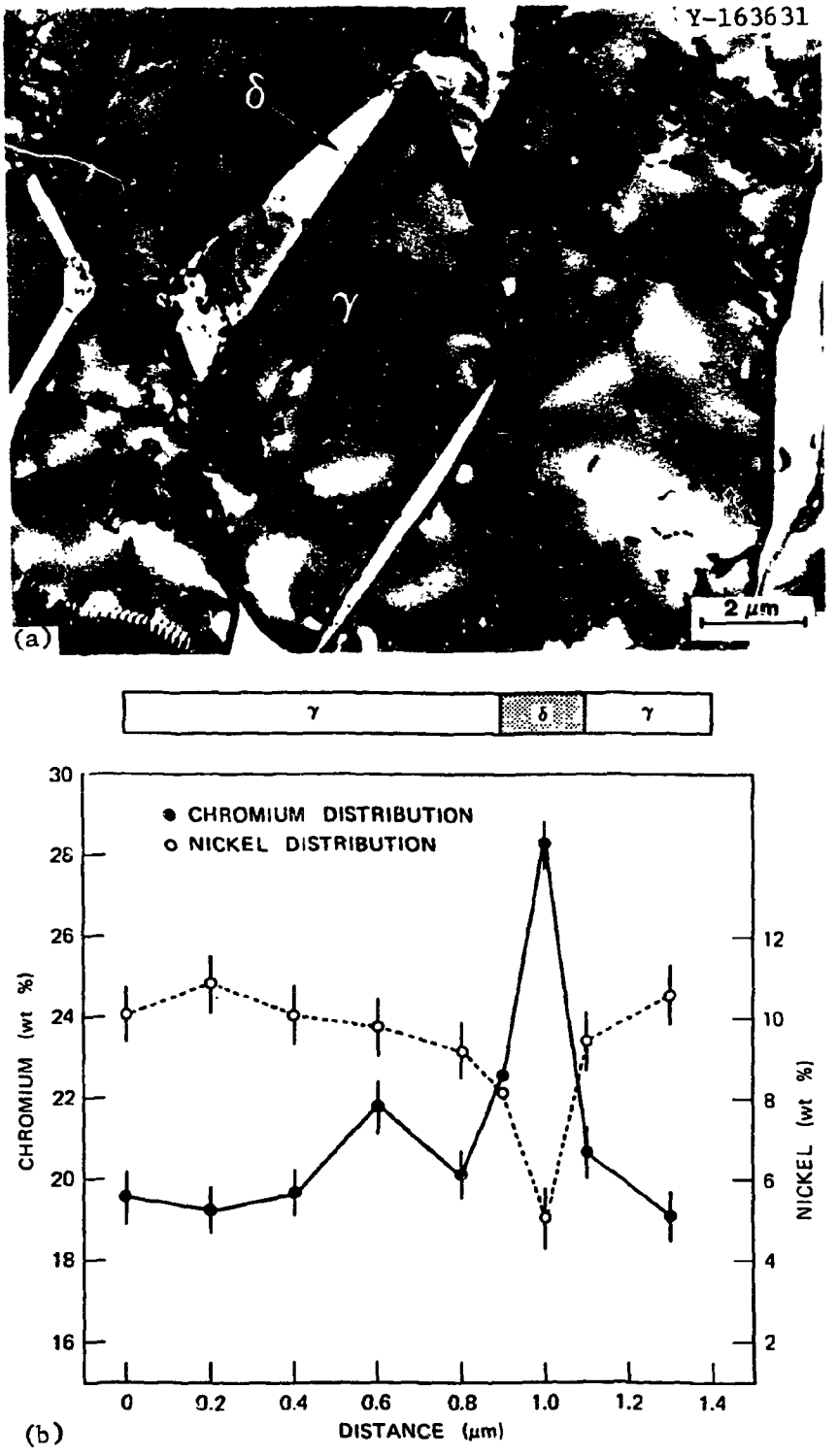

Fig. 8. Scanning Transmission Electron Microanalysis of δ-Ferrite in an Interrupted Solidification Sample. (a) Transmission electron micrograph. (b) Solute profile across the ferrite.

To correlate the results of the interrupted solidification experiments with welds, we made a GTA bead-on-plate weld with type 308 stainless steel filler metal. The sample was both microstructurally and STEM microanalyzed. An optical micrograph of a typical section of the weld is shown in Fig. 9. The microstructure shows regions typical of the skeletal network and acicular ferrite morphologies found in the interrupted solidification samples. Such variations in ferrite morphology within the weld depend on the variations in local solidification conditions. A transmission electron micrograph of a typical region analyzed by a STEM microanalyzer is shown in Fig. 10(a). Figure 10(b) shows the solute profile across ferrite in the weld sample. Here again the observed ferrite is finer. The average chromium and nickel contents in the austenite of the weld are 20 and 10 wt %, respectively, and in the ferrite 28 and 4 wt %. The solute profile within the ferrite and the composition of the ferrite in the weld appear similar to those of the interrupted solidification sample shown in Fig. 8. As in the interrupted solidification samples, diffusion seems to play an important role in the formation of the duplex structure in the weld.

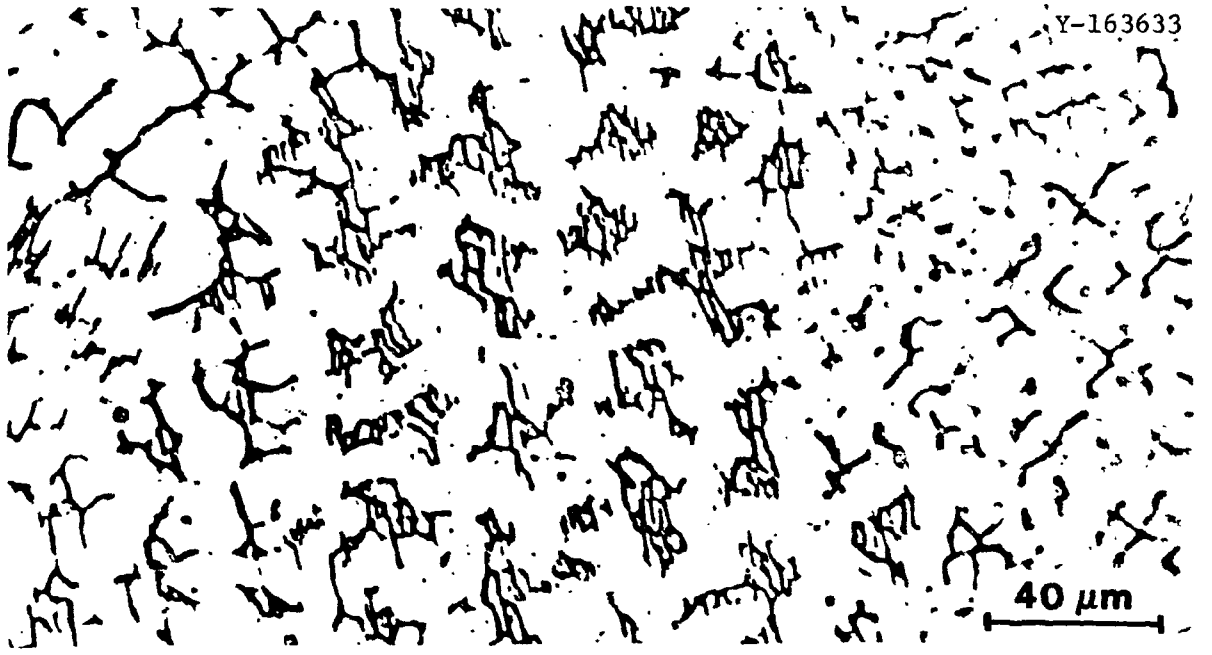

Fig. 9. A GTA Bead-on-Plate Weld with Type 308 Stainless Steel Filler Metal.

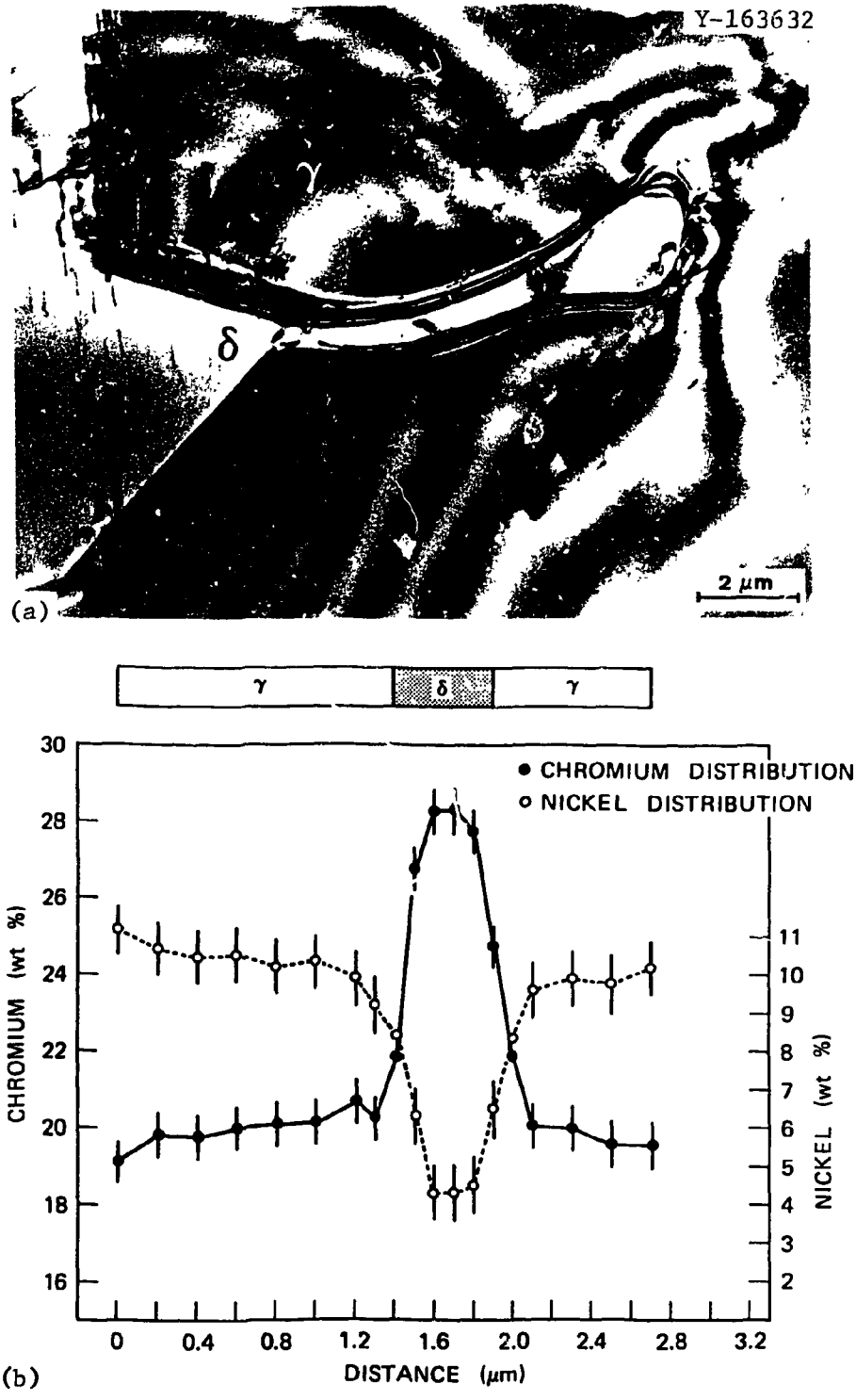

Fig. 10. Scanning Transmission Electron Microanalysis of Ferrite in the GTA Bead-on-Plate Weld. (a) Transmission electron micrograph. (b) Solute profile across the ferrite.

Solidification Microstructure of Type 310 Stainless Steel Filler Metal

As described earlier, solidification of type 310 stainless steel filler metal takes place with the primary formation of austenite. Figure 11 shows samples quenched from two temperatures below the liquidus. Primary austenite precipitates on cooling the sample to a temperature just below the liquidus [Fig. 11(a)]. The fine structure surrounding the primary phase indicates that the rest of the area was liquid at the moment of quenching. The volume fraction of the primary austenite continues to increase as the temperature decreases below the liquidus, leading to about 100% solid at a temperature of 1300°C [Fig. 11(b)]. During the above transformation of liquid to austenite the liquid is continuously enriched (partition ratio* $K_{Cr}^{\gamma-L} < 1$) in chromium. As solidification approaches completion, the last chromium-enriched liquid may solidify as δ-ferrite. The δ-ferrite would be located in the intercellular or interdendritic region. However, during this investigation no residual ferrite resulting from solute segregation at the intercellular or interdendritic regions was revealed by magnetic etching. The above observation compares well with a typical type 310 stainless steel weld, which, as shown in Fig. 12, is fully austenitic.

CONCLUSIONS

Interrupted solidification studies and differential thermal analysis aid in understanding weld metal microstructures.

The type 308 stainless steel filler metal investigated solidifies by the primary crystallization of δ-ferrite followed by austenite enveloping the ferrite. Depending on the cooling rate two modes of primary δ-ferrite transformation could take place, leading to the observed morphologies of the duplex structure. Thus, the ferrite in the duplex

---

*Equilibrium partition ratio $K_{Cr}^{\gamma-L} = C_{Cr}^{\gamma}/C_{Cr}^{L}$, where C_{Cr}^{γ} and C_{Cr}^{L} are the chromium contents of austenite and liquid given by the tie line at a particular temperature.

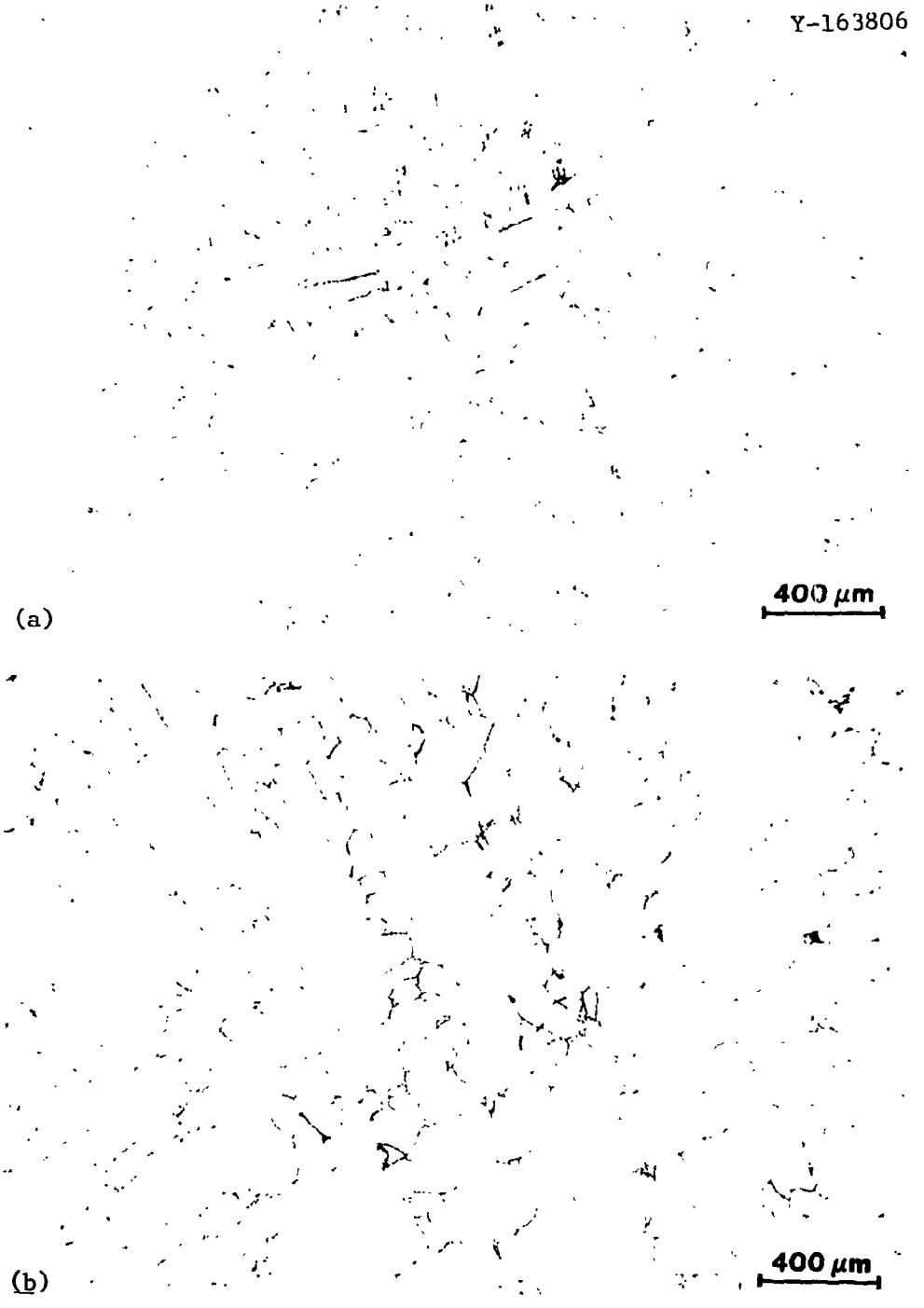

Fig. 11. Interrupted Solidification Samples of Type 310 Stainless Steel Filler Metal Quenched from (a) 1390°C and (b) 1300°C.

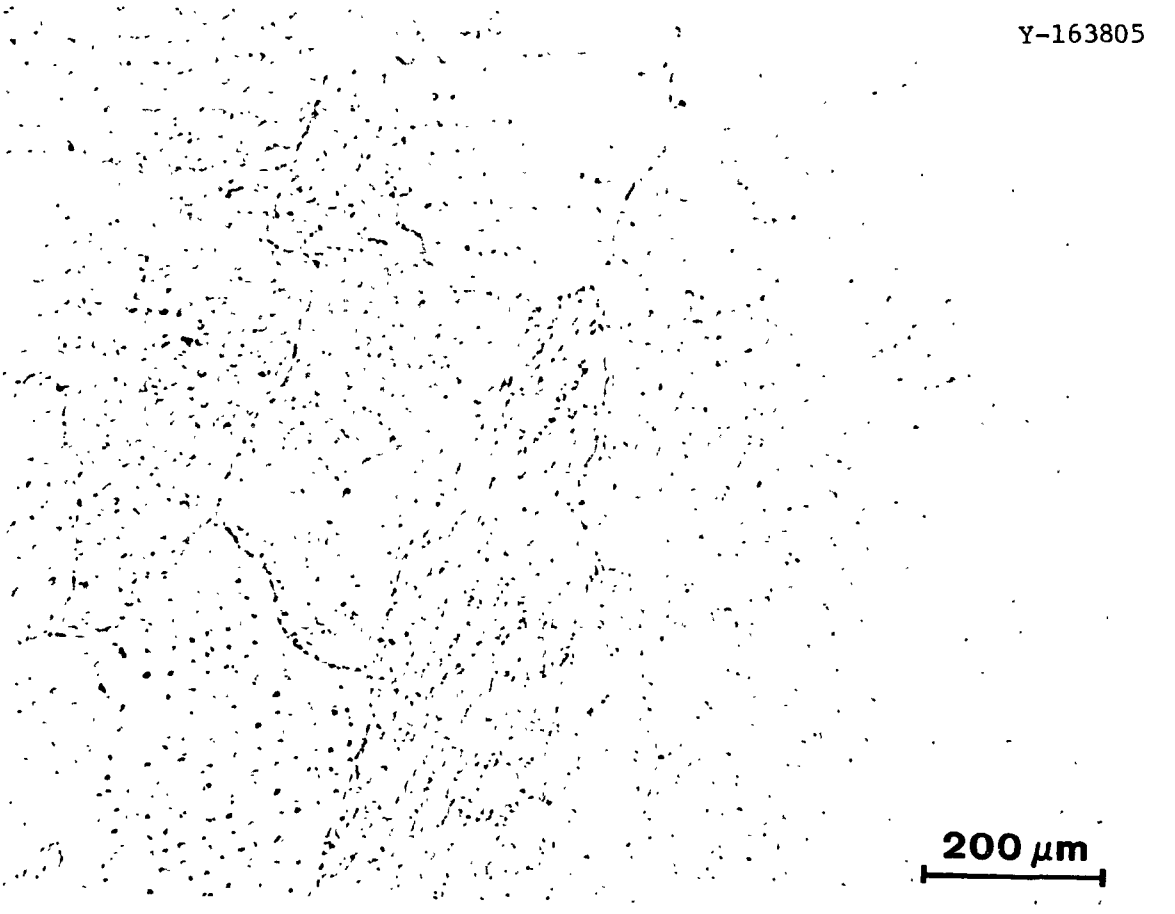

Fig. 12. A GTA Bead-on-Plate Weld with Type 310 Stainless Steel Filler Metal.

structure of the weld may be identified as (1) residual primary ferrite resulting from incomplete $\delta \rightarrow \gamma$ transformation or (2) residual ferrite after Widmanstätten austenite precipitation. During the above transformations solute redistributes extensively, leading to enrichment of ferrite in chromium and to depletion in nickel. This high level of chromium seems to stabilize the ferrite.

The type 310 stainless steel filler metal investigated solidifies by the primary crystallization of austenite with the transformation going to completion at the solidus temperature. In the samples residual ferrite was absent at the intercellular or interdendritic regions. This agrees with our observations on the type 310 stainless steel weld as well.

ACKNOWLEDGMENTS

The authors wish to acknowledge C. J. Long and V. B. Baylor for their helpful technical and editorial suggestions. We also acknowledge R. J. Gray, R. S. Crouse, and C. P. Haltom for their assistance in magnetic etching, microprobe analysis, and metallography, respectively. The report was edited by Sig Peterson and prepared for final publication by Shirley Frykman.

REFERENCES

1. A. L. Schaeffler, "Constitution Diagram for Stainless Steel Weld Metal," *Met. Prog.* 56: 680–680B (1949).
2. W. T. DeLong, G. A. Ostrom, and E. R. Szumachowski, "Measurement and Calculation of Ferrite in Stainless Steel Weld Metal," *Weld. J. (New York)* 35(11):521-s–528-s (1956).
3. W. T. DeLong, "Ferrite in Austenitic Stainless Steel Weld Metal," *Weld. J. (Miami)* 53(7): 273-s–286-s (1974).
4. S. A. David and G. M. Goodwin, "Solidification Behavior of Type 308 Stainless Steel Filler Metal," paper presented at Fifth Bolton Landing Conference, Lake George, New York, August 1978 (proceedings to be published).
5. J. C. Borland and R. N. Younger, "Some Aspects of Cracking in Austenitic Steels," *Br. Weld. J.* 7(1): 22–60 (1960).
6. F. C. Hull, "Effect of Delta Ferrite on the Hot Cracking of Stainless Steel," *Weld. J. (New York)* 46(9): 399-s–409-s (1967).
7. Y. Arata, F. Matsuda, and S. Katayama, "Solidification Crack Susceptibility in Weld Metals of Fully Austenitic Stainless Steel (Report I) — Fundamental Investigation on Solidification Behavior of Fully Austenitic and Duplex Microstructures and Effect of Ferrite on Microsegregation," *Trans. JWRI* 5(2): 35–51 (1976).
8. P. P. Puzak, W. R. Apblett, and W. S. Pellini, "Hot Cracking of Stainless Steel Weldments," *Weld. J. (New York)* 35(1): 9-s–17-s (1956).

9. W. S. Pellini, "Strain Theory of Hot Tearing," *Foundry* 80: 125 (November 1952).

10. W. R. Apblett, and W. S. Pellini, "Factors Which Influence Weld Hot Cracking," *Weld. J. (New York)* 33(2): 83-s–90-s (1954).

11. J. C. Borland, "Generalized Theory of Super-Solidus Cracking in Welds (and Castings)," *Br. Weld. J.* 7(8): 508–12 (1960).

12. I. Masumoto, K. Tamaki, and M. Kutsuma, "Hot Cracking of Austenitic Steel Weld Metal," *Yosetsu Gakkai-Shi*, 41(11): 1306–14 (1972).

13. H. Astrom et al., "Hot Cracking and Micro-Segregation in 18-10 Stainless Steel Welds," *Met. Sci.* 10(7), 225–34 (1976).

14. C. E. Lyman et al., "STEM Microanalysis of Duplex Stainless Steel Weld Metal," *Scanning Electron Micros.* 1: 213–34 (1976).

15. G. Cliff and G. W. Lorimer, *Electron Micros. Proc. Eur. Congr. 5th, 1972, Inst. Phys. Conf. Ser.* n14, London, pp. 140–41

16. H. Fredriksson, "The Solidification Sequence in an 18-8 Stainless Steel, Investigated by Directional Solidification," *Metall. Trans.* 3(11): 2989–97 (1972).